Current Optics and Photonics
Vol. 4, No. 5, October 2020, pp. 434-440

ISSN: 2508-7266(Print) / ISSN: 2508-7274(Online)
DOI: https://doi.org/10.3807/COPP.2020.4.5.434

Circuit Model for the Effect of Nonradiative Recombination in a High-Speed Distributed-Feedback Laser

Bowen Nie[1], Zhijuan Chi[2], Qing-an Ding[1]*, Xiang Li[1], Changqing Liu[1], Xiaojuan Wang[1], Lijun Zhang[1], Juan Song[1], and Chaofan Li[1]

[1]*College of Electronic and Information Engineering, Shandong University of Science and Technology, Qingdao 266590, China*
[2]*College of Foreign Languages, Qingdao Binhai University, Qingdao 266590, China*

(Received May 11, 2020 : revised July 28, 2020 : accepted August 25, 2020)

Based on single-mode rate equations, we present an improved equivalent-circuit model for distributed-feedback (DFB) lasers that accounts for the effects of parasitic parameters and nonradiative recombination. This equivalent-circuit model is composed of a parasitic circuit, an electrical circuit, an optical circuit, and a phase circuit, modeling the circuit equations transformed from the rate equations. The validity of the proposed circuit model is verified by comparing simulation results to measured results. The results show that the slope efficiency and threshold current of the model are 0.22 W/A and 13 mA respectively. It is also shown that increasing bias current results in the increase of the relaxation-oscillation frequency. Moreover, we show that the larger the bias current, the lower the frequency chirp, increasing the possibility of extending the transmission distance of an optical-fiber communication system. The results indicate that the proposed circuit model can accurately predict a DFB laser's static and dynamic characteristics.

Keywords : Chirp characteristics, Distributed feedback laser, Equivalent circuit model, Nonradiative recombination, Rate equations
OCIS codes : (140.3490) Lasers, distributed-feedback; (230.0250) Optoelectronics; (250.5960) Semiconductor lasers

I. INTRODUCTION

Distributed-feedback (DFB) lasers are widely used in the fields of modern optical communication, high-speed information transmission, due to their low power consumption, high modulation bandwidth, narrow spectrum width, and satisfactory single-mode characteristics [1-6]. Presently there are many sophisticated physical models [7, 8], numerical simulation approaches [9, 10], and computer programs [11] that can accurately indicate a DFB laser's output characteristics. Compared to these numerical methods of high computational complexity, optoelectronic integrated circuit computer-aided design (OEIC CAD) is more succinct and effective. It achieves the goal of optimizing device design by establishing an equivalent-circuit model of an optoelectronic device, and simulating the model to analyze various characteristics of the device. Recently many equivalent-circuit models have been proposed to analyze laser output behavior, including the small-signal equivalent-circuit model for photonic crystal Fano lasers [12], the equivalent-circuit model for dual-wavelength quantum cascade lasers [13], and the noise equivalent-circuit model for semiconductor lasers [14]. Among the papers investigating DFB lasers, most of them have only focused on analyzing and modeling two basic rate equations [15-17], and at least one effect has been neglected, such as package parasitics, nonradiative recombination, or phase information.

In this paper, the nonradiative-recombination and phase rate equations for DFB lasers are introduced, from which an improved equivalent-circuit model is proposed. The model presented in this paper can be easily implemented using

*Corresponding author: aqd6677@126.com, ORCID 0000-0003-4850-2846
Color versions of one or more of the figures in this paper are available online.

circuit-simulation software, such as PSpice. The software can simulate dc bias characteristics, large-signal pulse modulation response, and small-signal frequency response. Furthermore, compared to other circuit models [15-17], this model is established with the phase rate equation, which enables us to investigate the frequency-chirp characteristics of DFB lasers. Because the model considers the effect of nonradiative recombination, there is great value in applying the model for analyzing and improving the physical design of DFB lasers. In addition, the transmission distance of an optical-fiber communication system can be extended by suppressing the frequency chirp of DFB lasers.

This paper is organized in five parts. In Section II, we transform the rate equations for a DFB laser into the corresponding circuit equations. In Section III, the complete circuit model for a DFB laser is described. Accordingly, the parameters of the circuit model are listed. The static and dynamic responses of a DFB laser are analyzed in Section IV, and the simulation results for the circuit model are compared to measured results from [18, 19]. Finally, the conclusion is presented in Section V.

II. CIRCUIT EQUATIONS FOR A DFB LASER

The starting point for establishing a DFB laser's equivalent-circuit model is the rate equations that describe its electro-optical characteristics. The single-mode rate equations for a DFB laser can be written as [18]

$$\frac{dN}{dt}=\frac{I_j}{qV}-R_n(N)-R_r(N)-\frac{g_0(N-N_0)}{1+\varepsilon S}S, \tag{1}$$

$$\frac{dS}{dt}=\Gamma\frac{g_0(N-N_0)}{1+\varepsilon S}S+\Gamma\beta R_r(N)-\frac{S}{\tau_p}, \tag{2}$$

$$\frac{d\phi}{dt}=\frac{1}{2}\alpha\left[\Gamma g_0(N-N_0)-\frac{1}{\tau_p}\right], \tag{3}$$

where N is the active-region carrier density, I_j is the injection current, $R_n(N)$ is the rate of nonradiative recombination, q is an electron's charge, V is the active-layer volume, $R_r(N)$ is the rate of radiative recombination, S is the photon density, Γ is the optical-confinement factor, ε is the optical-gain-compression factor, N_0 is the transparent-carrier concentration, β is the spontaneous-emission factor, ϕ is the output optical phase, τ_p is the photon lifetime, g_0 is the gain coefficient, and α is the linewidth-enhancement factor. In the analysis of these rate equations, the rate of nonradiative recombination is expressed as [19]

$$R_n(N)=A_{n1}N+A_{n2}N^2+A_{n3}N^3, \tag{4}$$

where A_{n1} is the deep-level-recombination coefficient, and A_{n2} and A_{n3} are the low-level- and high-level-injection Auger-recombination coefficients respectively. The rate of radiative recombination is given by [19]

$$R_r(N)=A_{r1}N+A_{r2}N^2, \tag{5}$$

where A_{r1} and A_{r2} are the low-level- and high-level-injection radiative-recombination coefficients respectively.

With the Shockley relationship $N=N_e\left[\exp\left(V_j/2V_T\right)-1\right]$ substituted [20], Eq. (1) becomes

$$I_j=C_d\frac{dV_j}{dt}+I_n+I_r+I_{st}, \tag{6}$$

where C_d is the junction diffusion capacitance, and I_n, I_r, and I_{st} are the nonradiative-recombination current, radiative-recombination current and stimulated-emission current respectively. They are modeled as dependent current generators (controlled by N, or N and S). Their expressions are given by

$$C_d=\frac{qVN_e}{2V_T}\exp\left(\frac{V_j}{2V_T}\right),$$

$$I_n=qVR_n(N),$$

$$I_r=qVR_r(N),$$

$$I_{st}=qV\frac{g_0(N-N_0)}{1+\varepsilon S}S,$$

in which V_j is the junction voltage, $V_T=kT/q$ is the thermal voltage, and N_e is the equilibrium carrier density. The space-charge capacitance C_{sc} is given by [19]

$$C_{sc}=C_0\left(1-\frac{V_j}{V_D}\right)^{-1/2},$$

where C_0 is the zero-bias junction capacitance and V_D is the built-in voltage. Eq. (6) (a circuit equation) and the space-charge capacitance can be represented by the circuit shown in Fig. 1.

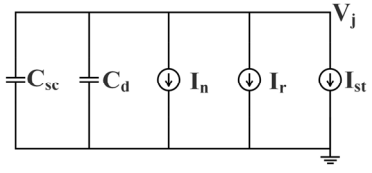

FIG. 1. Schematic diagram of the electrical circuit for a high-speed DFB laser's equivalent-circuit model.

Multiplied by qV on both sides, Eq. (2) can be changed to

$$\Gamma\beta I_r + \Gamma I_{st} = C_{ph}\frac{dV_{ph}}{dt} + \frac{V_{ph}}{R_{ph}}, \tag{7}$$

where $V_{ph} = SVV_T$ is the optical voltage, the current generator $\Gamma\beta I_r$ models the spontaneous radiation coupled into the laser mode, and photon loss and storage are modeled by the resistance $R_{ph} = V_T\tau_p/q$ and capacitance $C_{ph} = q/V_T$ respectively. The relationship between the optical output power and photon density satisfies [21]

$$P_{out} = \frac{SV\eta_0 h\nu}{2\Gamma\tau_p} = \frac{V_{ph}\eta_0 h\nu}{2\Gamma\tau_p V_T} = \xi V_{ph}, \tag{8}$$

where η_0 is the total quantum efficiency, ν is the laser frequency, and h is Planck's constant. The output power is a scaled analog of the optical voltage or photon density. From Eqs. (7) and (8), the optical circuit is shown in Fig. 2. Eqs. (6) and (7) are standard circuit equations; however, the phase information is not involved in those equations, so the frequency-chirp characteristics of a DFB laser cannot be illustrated with those circuits. Therefore, for the purpose of analyzing the frequency-chirp characteristics of a DFB laser, the phase circuit needs to be included in the circuit model.

The relation between the frequency chirp $\Delta\nu$ and output optical phase is expressed as [22]

$$\Delta\nu = \frac{1}{2\pi}\frac{d\phi}{dt} = \frac{1}{4\pi}\alpha\left[\Gamma g_0(N - N_0) - \frac{1}{\tau_p}\right]. \tag{9}$$

With these definitions' help

$$V_{chirp} = \Delta\nu\tau_p V_T,$$

$$R_{chirp} = \frac{V_T\tau_p}{q},$$

$$I_{chirp} = \frac{1}{4\pi}\alpha q\left[\Gamma g_0(N - N_0) - \frac{1}{\tau_p}\right].$$

Eq. (9) can be rewritten as

$$I_{chirp} = \frac{V_{chirp}}{R_{chirp}}, \tag{10}$$

and the expression for the frequency chirp becomes

$$\Delta\nu = \frac{V_{chirp}}{V_T\tau_p} = \xi' V_{chirp}. \tag{11}$$

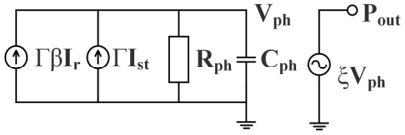

FIG. 2. Schematic diagram of the optical circuit for a high-speed DFB laser's equivalent-circuit model.

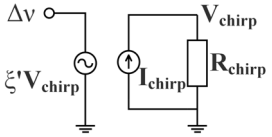

FIG. 3. Schematic diagram of the phase circuit for a high-speed DFB laser's equivalent-circuit model.

The frequency chirp is modeled as a voltage generator, and is proportional to V_{chirp}. The phase circuit is shown in Fig. 3.

III. IMPROVED EQUIVALENT-CIRCUIT MODEL FOR A DFB LASER

With Eqs. (6), (7), (8), (10), and (11) derived, the equivalent-circuit model for a DFB laser can be established. The model consists of four parts: a parasitic circuit, electrical circuit, optical circuit, and phase circuit. In Fig. 4, R_d is the bleeder resistance, C_p is the parasitic shunt capacitance, and R_s is the series resistance.

The model is implemented using Cadence's PSpice software. We use the dot command, like a script language, to define every component of the model, such as the resistances, capacitances, current sources, etc. The circuit-model diagrams shown in Fig. 4 can help the reader to understand the model intuitively. Actually, unlike the circuit diagrams, the model is composed of many dot commands. Table 1 lists the major parameters [18, 23] applied in the circuit-model simulation of Fig. 4.

As discussed in Section II, the complete circuit model consisting of four subcircuits can be modeled by Eqs. (6), (7), (8), (10), and (11), according to Kirchhoff's Circuit Law. We simulate this equivalent-circuit model using the software PSpice, and compare the simulation results to data obtained from [18, 19]. The flow diagram for simulating the circuit model for a DFB laser is show in Fig. 5. The process of simulating the circuit model is as follows: First, as demonstrated in Section II, we transform the rate equations for the DFB laser into circuit equations. Second, we establish the circuit model based on the circuit equations, as shown in Fig. 4. Then we define the expressions for the circuit-model elements, the constants, and parameters of the rate equations, such as the nonradiative-recombination current source I_n, the electron's charge q, the carrier lifetime τ_n, etc. Next we compile the dot commands

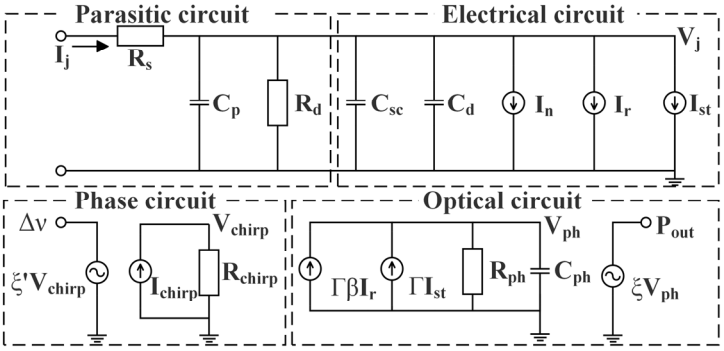

FIG. 4. Schematic diagram of the improved equivalent-circuit model for a high-speed DFB laser.

TABLE 1. Parameter values for the DFB laser

Symbol	Description	Value
V	Active-layer volume	1.78×10^{-11} cm^3
Γ	Mode-confinement factor	0.25
g_0	Gain-slope constant	1.42×10^{-6} cm^3/s
η_0	Differential quantum efficiency	0.2
ε	Gain-compression factor	1.32×10^{-17} cm^3
τ_p	Photon lifetime	0.76 ps
β	Spontaneous-emission factor	9.0×10^{-5}
N_0	Carrier density for transparency	9.3×10^{17} cm^{-3}
A_{n1}	Deep-level-recombination coefficient	1.0×10^8 s^{-1}
A_{n2}	Low-level-injection Auger-recombination coefficient	1.1×10^{-17} m^3 s^{-1}
A_{n3}	High-level-injection Auger-recombination coefficient	2.0×10^{-41} m^6 s^{-1}
A_{r1}	Low-level-injection radiative-recombination coefficient	4.2×10^8 s^{-1}
A_{r2}	High-level-injection radiative-recombination coefficient	1.5×10^{-16} m^3 s^{-1}

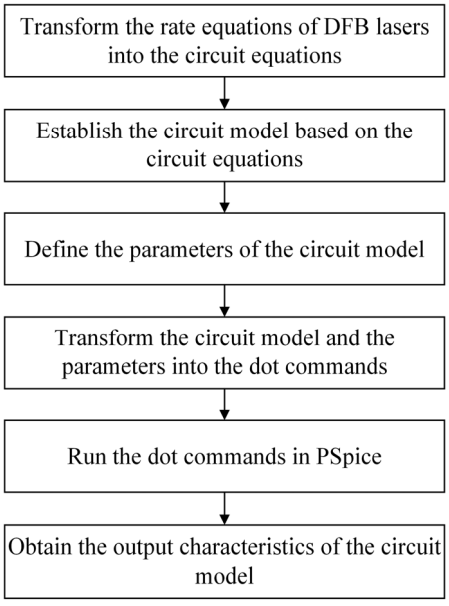

FIG. 5. Flow diagram for simulating the circuit model for a high-speed DFB laser.

for the circuit-model elements, the constants, and the parameters of the rate equations. Finally, we run the dot commands in PSpice and obtain the output-characteristic diagrams for the model, as shown in Section IV.

IV. RESULTS AND DISCUSSION

In this section, we simulate the high-speed DFB laser via PSpice. In doing so, we first run the dot commands transformed from the circuit Eqs. (6), (7), (8), (10), and (11) in PSpice and predict the high-speed DFB laser's output characteristics. Then, for the sake of comparison, we quote the data obtained from [18, 19].

The circuit model is driven from an ideal current source increased from 0 mA to 80 mA in steps of 0.1 mA. The simulated *P-I* curve of the DFB laser's circuit model is depicted in Fig. 6. As the injection current increases, the output optical power also increases, but it is not a simple linear relationship. As the injection current increases beyond the threshold current, the output optical power increases

sharply. When the injection current is below the threshold, the laser emits light with a very wide spectrum and poor coherence. In practical applications gain saturation occurs during laser operation, *i.e.* when the bias current reaches a certain value, the output optical power is no longer linear in the bias current. The conversion efficiency of a DFB laser is often measured by the slope efficiency, which is the slope of the laser's *P-I* curve above the threshold. As seen from Fig. 6, the slope efficiency is 0.22 W/A and the threshold current is 13 mA. It can also be shown that the simulated results agree well with measured results obtained from [18]. Thus the improved equivalent-circuit model can accurately simulate the dc-bias characteristics of a DFB laser.

The small-signal frequency-response characteristics determine the highest modulation frequency of a DFB laser, which is represented by the 3-dB bandwidth. Figure 7 illustrates the simulated and measured small-signal frequency response at three bias levels [23]. In direct modulation, the relationship between the output power of the DFB laser and the modulation frequency is given by

$$P(f)=\frac{P(0)}{\sqrt{[1-(f/f_r)^2]^2+4\gamma^2(f/f_r)^2}}, \tag{12}$$

where f_r is the relaxation-oscillation frequency, and γ is the damping factor. The optical output power near the relaxation frequency will be higher than the output power at other frequencies. When the laser bias current is above the threshold and the modulation signal is small enough, the 3-dB modulation bandwidth of the DFB laser can be approximately expressed as [24]

$$f_{3dB}=\left[\frac{3G_N\eta_{\text{int}}}{4\pi^2 qV}(I_0-I_{th})\right]^{1/2}. \tag{13}$$

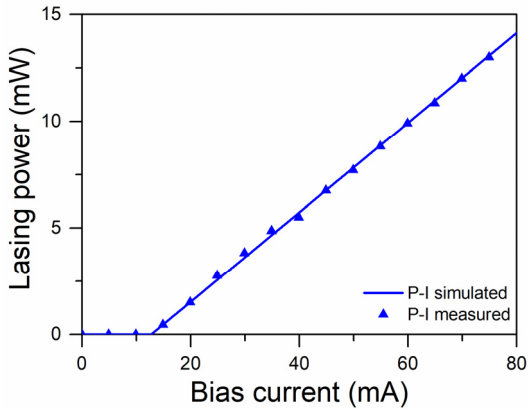

FIG. 6. Lasing power from the high-speed DFB laser's equivalent-circuit model, versus the bias current. The line depicts the circuit-model simulation results, and triangles stand for published data from [18].

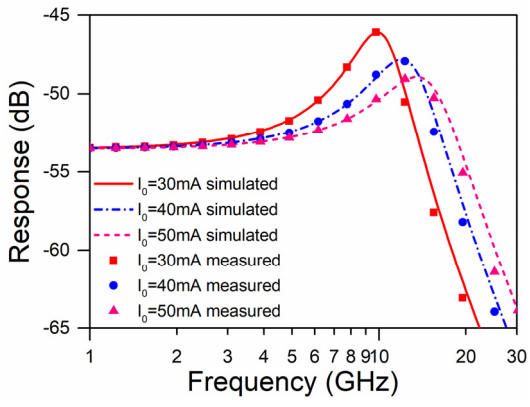

FIG. 7. Small-signal frequency response of the equivalent-circuit model for a high-speed DFB laser at various bias currents: I_0 = 30 mA (solid line), 40 mA (dot-dashed), and 50 mA (dashed). Lines depict the model simulation results, while squares, circles, and triangles represent data obtained from [19].

As shown in Fig. 7, the curves are flat at low frequency, and with the modulation frequency close to the relaxation-oscillation frequency the modulation response distorts. Moreover, the modulation response decreases rapidly when the modulation frequency continues to grow. For a bias current of 30 mA, the 3-dB bandwidth is about 9 GHz; for a bias current of 50 mA, the 3-dB bandwidth is about 12 GHz. Thus the 3-dB bandwidth increases with increasing bias current. However, increasing the bias current without limit can lead to self-pulsation. The consistency of the measured and simulated results demonstrates that the model is of great value in simulating and analyzing DFB lasers.

Most DFB lasers in an optical-fiber communication system are in the state of large-signal modulation, so it is necessary to analyze the large-signal pulse-modulation response of a DFB laser. The circuit model is driven by an ideal current source in the pulsed mode of operation; its parameters are shown in Table 2. It can be seen from Fig. 8 that there is relaxation oscillation in the rising edge, and overshoot in the falling edge, of the pulse response. This phenomenon is the inherent characteristic of electro-optical interaction in DFB lasers. There also tends to be a decrease of relaxation time and amplitude with increasing bias current, because of the gain-saturation effect in DFB lasers. Additionally, the output optical power increases with increasing bias current, due to the increase of the number of carriers in the active region of the laser, resulting in more photons produced by the stimulated recombination.

The *frequency chirp* of a DFB laser means that the output optical frequency varies with time; in other words, the output optical phase changes over time. The circuit model is also driven by an ideal current source, with parameters shown in Table 2. In pulse modulation, the chirp can be divided into the *transient chirp* and the *adiabatic chirp*. The relaxation oscillation of optical frequency after a current jumps is defined as the transient chirp; the stable

TABLE 2. Parameter values for the current source

Parameter	Quantity	Unit
I_{low}	40	mA
I_{high}	60	mA
Rise time	0	ns
Fall time	0	ns
Delay	1	ns
Width	1	ns
Period	3	ns

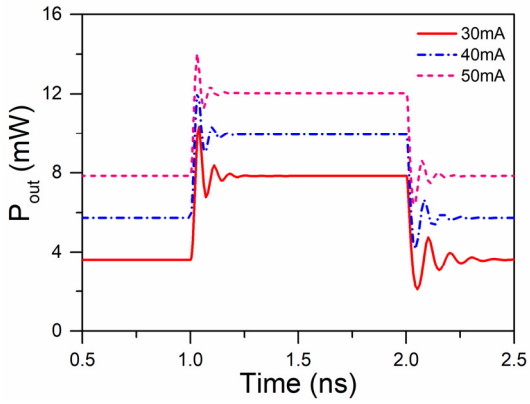

FIG. 8. Optical output power versus time from the high-speed DFB laser's equivalent-circuit model, at various bias currents: I_0 = 30 mA (solid line), 40 mA (dot-dashed), and 50 mA (dashed).

optical frequency after the relaxation oscillation disappears is defined as the adiabatic chirp. The expression for the frequency chirp is written as

$$\Delta\nu(t) \cong \frac{\alpha}{4\pi}\left(\frac{d}{dt}\ln P(t) + \kappa P(t)\right), \tag{14}$$

where $\kappa = 2\Gamma\varepsilon/V\eta h\upsilon$. The first term in Eq. (15) is the transient chirp, determined by the rate of change of the output power, and the second term is the adiabatic chirp, which is proportional to the steady-state value of the output power; the proportionality factor is κ. To illustrate the frequency chirp clearly, we use an expression that differs from Eq. (9), but both expressions for the chirp possess the same physical meaning. With regard to the direct-modulation laser, the frequency chirp leading to spectral expansion and then shortening of the transmission distance has been one of the major factors that limit laser performance. As Fig. 9 shows, the adiabatic chirp at various currents is always about 4 GHz, and the transient chirp decreases with increasing bias currents. This indicates that increasing the bias current can effectively suppress the transient chirp of the laser, and reduce the frequency chirp. Therefore we can conclude that increasing the bias current

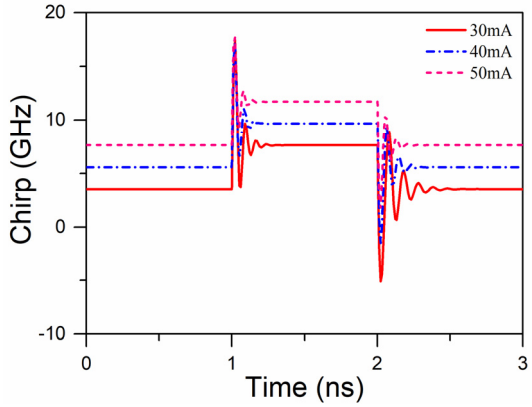

FIG. 9. Frequency chirp versus time from the high-speed DFB laser's equivalent-circuit model. at various bias currents: I_0 = 30 mA (solid line), 40 mA (dot-dashed), and 50 mA (dashed).

provides the possibility to extend the transmission distance of DFB lasers.

V. CONCLUSION

In this paper an improved circuit-simulation model for DFB lasers, considering the effects of parasitic parameters and nonradiative recombination, was presented. The proposed model consisted mainly of three coupled electrical circuits. The simulation results obtained by modeling the circuit equations via PSpice were compared to measured results obtained from [18, 19]. The comparison shows good agreement between both sets of results, demonstrating that the presented model can provide great reference value in describing a high-speed DFB laser's output characteristics. Moreover, the static and dynamic characteristics of a high-speed DFB laser were simulated using the model. The simulation results showed that a high-speed DFB laser can be modulated at frequencies of about 12 GHz by increasing the bias current. Furthermore, it was also shown that frequency chirp can be decreased by increasing the bias current. All of the simulation results indicated that the proposed model can be a very useful tool for predicting and analyzing the operating characteristics of DFB lasers.

ACKNOWLEDGMENT

This work was supported by Shandong Natural Science Foundation, China (No. ZR2017MF070), National Natural Science Foundation of China (No. 61471224), Scientific Research Foundation of Shandong University of Science and Technology for Recruited Talents (No. 2016RCJJ012), and the Domestic Visiting Scholar supported by Shandong University of Science and Technology.

REFERENCES

1. S. Kanazawa, W. Kobayashi, Y. Ueda, T. Fujisawa, K. Takahata, T. Ohno, T. Yoshimatsu, H. Ishii, and H. Sanjoh, "30-km error-free transmission of directly modulated DFB laser array transmitter optical sub-assembly for 100-Gb application," J. Lightwave Technol. **34**, 3646-3652 (2016).
2. Z. Deng, J. Li, M. Liao, W. Xie, and S. Luo, "InGaN/GaN distributed feedback laser diodes with surface gratings and sidewall gratings," Micromachines **10**, 699 (2019).
3. M. Chen, S. Liu, Y. Shi, P. Dai, Y. Zhao, Y. Xu, T. Fang, J. Lu, B. Yang, and X. Chen, "Study on DFB semiconductor laser based on sampled moiré grating integrated with grating reflector," IEEE J. Quantum Electron. **56**, 2200109 (2020).
4. F. Vogelbacher, M. Sagmeister, J. Kraft, X. Zhou, J. Huang, M. Li, K. J. Jiang, Y. Song, K. Unterrainer, and R. Hainberger, "Slot-waveguide silicon nitride organic hybrid distributed feedback laser," Sci. Rep. **9**, 18438 (2019).
5. K. Guo, J. He, K. Yang, Z. Zhang, X. Xu, B. Du, G. Xu, and Y. Wang, "Symmetric step-apodized distributed feedback fiber laser with improved efficiency," IEEE Photonics J. **11**, 1600211 (2019).
6. R. Y. Chen, Y. J. Chen, C. L. Chen, C. C. Wei, W. Lin, and Y. J. Chiu, "High-power long-waveguide 1300-nm directly modulated DFB laser for 45-Gb/s NRZ and 50-Gb/s PAM4," IEEE Photonics Technol. Lett. **30**, 2091-2094 (2018).
7. Y. Chung, "Split-step time-domain modeling of dual-mode DFB laser diode for terahertz wave generation," Microw. Opt. Technol. Lett. **61**, 1895-1900 (2019).
8. A. Ghadimi and S. Alikhah, "Simulation and analysis of dependence of threshold current and gain of λ/4 shifted DFB laser through transfer matrix," J. Opt. **46**, 479-485 (2017).
9. P. Salík and R. Róka, "Analysis of possibilities for numerical simulations of continuous wave DFB laser," in *Proc. International Congress on Ultra Modern Telecommunications and Control Systems and Workshops* (Munich, Germany, Nov. 2017), pp. 215-219.
10. I. Fatadin, D. Ives, and M. Wicks, "Numerical simulation of intensity and phase noise from extracted parameters for CW DFB lasers," IEEE J. Quantum Electron. **42**, 934-941 (2006).
11. P. Vankwikelberge, G. Morthier, and R. Baets, "CLADISS-a longitudinal multimode model for the analysis of the static, dynamic, and stochastic behavior of diode lasers with distributed feedback," IEEE J. Quantum Electron. **26**, 1728-1741 (1990).
12. A. R. Zali, M. K. Moravvej-Farshi, and M. H. Yavari, "Small-signal equivalent circuit model of photonic crystal fano laser," IEEE J. Sel. Top. Quantum Electron. **25**, 4900108 (2019).
13. M. Darman and K. Fasihi, "An equivalent circuit-level model for dual-wavelength quantum cascade lasers," Optik **136**, 428-434 (2017).
14. M. Darman and K. Fasihi, "A new compact circuit-level model of semiconductor lasers: investigation of relative intensity noise and frequency noise spectra," J. Mod. Opt. **64**, 1839-1845 (2017).
15. S. J. Zhang, N. H. Zhu, E. Y. B. Pun, and P. S. Chung, "Rate-equation-based circuit model of high-speed semiconductor lasers," Microw. Opt. Technol. Lett. **49**, 539-542 (2007).
16. R. Borras, J. del Rio, C. Oriach, and J. Juliachs, "Laser diodes optical output power model," Measurement **133**, 56-67 (2019).
17. M. Darman and K. Fasihi, "A new compact circuit-level model of semiconductor lasers: investigation of relative intensity noise and frequency noise spectra," J. Mod. Opt. **64**, 1839-1845 (2017).
18. J. C. Cartledge and R. C. Srinivasan, "Extraction of DFB laser rate equation parameters for system simulation purposes," J. Lightwave Technol. **15**, 852-860 (1997).
19. W. Y. Chen, S. R. Yang, and S. Liu, *Optoelectronic devices circuit model and the circuit-level simulation of OEIC* (National Defense Industry Press, Beijing, CN, 2001), Chapter 2.
20. R. Tucker and D. Pope, "Circuit modeling of the effect of diffusion on damping in a narrow-stripe semiconductor laser," IEEE J. Quantum Electron. **19**, 1179-1183 (1983).
21. L. Bjerkan, A. Royset, L. Hafskjaer, and D. Myhre, "Measurement of laser parameters for simulation of high-speed fiberoptic systems," J. Lightwave Technol. **14**, 839-850 (1996).
22. J. C. Cartledge and G. S. Burley, "The effect of laser chirping on lightwave system performance," J. Lightwave Technol. **7**, 568-573 (1989).
23. T. T. Shih, M. C. Lin, and W. H. Cheng, "High-performance low-cost 10-Gb/s coaxial DFB laser module packaging by conventional TO-Can materials and processes," IEEE J. Sel. Top. Quantum Electron. **12**, 1009-1016 (2006).
24. L. Bjerkan, A. Royset, L. Hafskjaer, and D. Myhre, "Measurement of laser parameters for simulation of high-speed fiberoptic systems," J. Lightwave Technol. **14**, 839-850 (1996).